Enhanced Performance of Fullerene n-Channel Field-Effect Transistors with Titanium Sub-Oxide Injection Layer

By *Shinuk Cho,* Jung Hwa Seo, Kwanghee Lee,** and *Alan J. Heeger**

Enhanced performance of n-channel organic field-effect transistors (OFETs) is demonstrated by introducing a titanium sub-oxide (TiO_x) injection layer. The n-channel OFETs utilize [6,6]-phenyl-C_{61} butyric acid methyl ester ($PC_{61}BM$) or [6,6]-phenyl-C_{71} butyric acid methyl ester ($PC_{71}BM$) as the semiconductor in the channel. With the TiO_x injection layer, the electron mobilities of $PC_{61}BM$ and $PC_{71}BM$ FET using Al as source/drain electrodes are comparable to those obtained from OFETs using Ca as the source/drain electrodes. Direct measurement of contact resistance (R_c) shows significantly decreased R_c values for FETs with the TiO_x layer. Ultraviolet photoelectron spectroscopy (UPS) studies demonstrate that the TiO_x layer reduces the electron injection barrier because of the relatively strong interfacial dipole of TiO_x. In addition to functioning as an electron injection layer that eliminates the contact resistance, the TiO_x layer acts as a passivation layer that prevents penetration of O_2 and H_2O; devices with the TiO_x injection layer exhibit a significant improvement in lifetime when exposed to air.

1. Introduction

Because of their excellent electron transport properties and good processability, the soluble fullerenes [6,6]-phenyl-C_{61} butyric acid methyl ester ($PC_{61}BM$) and [6,6]-phenyl-C_{71} butyric acid methyl ester ($PC_{71}BM$) have received considerable attention as semiconductors for n-channel organic field-effect transistors (OFETs).[1–6] Electron mobilities as high as 0.1 $cm^2\ V^{-1}\ s^{-1}$ have been demonstrated.[4,5]

There are two major constraints that need to be overcome to maximize n-channel performance: i) Electron trapping by hydroxyl group at the semiconductor-dielectric interface; ii) Poor injection of electrons from the drain electrode into the active layer. The former can be overcome by using hydroxyl-free polymer dielectric materials.[5,7–8] For example, a divinyltetramethylsiloxane-bis (benzocyclobutene) derivative (BCB) as the gate dielectric material yields an electron-trap-free interface.[7] Good electron injection can be achieved by using low work function metals such as Ca and Mg. These low work function metals are, however, air-sensitive with associated degradation of device performance. LiF has been used as an electron injection layer to achieve better electron injection from Al or Ag.[8–11] Because of the difficulties involved in fabricating the required ultra-thin LiF layers (<1 nm), this approach is not attractive for low-cost OFET devices.

In this paper, we demonstrate reduced contact resistance and relatively high field-effect mobility in n-channel OFETs based on the soluble fullerenes $PC_{61}BM$ and $PC_{71}BM$. Improved injection is achieved by introducing an electron injection layer using solution processible titanium sub-oxide (TiO_x). The mobilities obtained from FETs with Al electrodes and the TiO_x injection layer approach the values obtained using Ca as source/drain electrodes. Ultraviolet photoelectron spectroscopy (UPS) measurements demonstrate that the TiO_x injection layer reduces the barrier for electron injection, thereby reducing the contact resistance. In addition to working as the electron injection layer, the TiO_x layer functions as a passivation layer that prevents penetration of O_2 and H_2O; devices with the TiO_x injection layer exhibit a significant improvement in lifetime when exposed to air.

2. Results and Discussion

The molecular structures of $PC_{61}BM$ and $PC_{71}BM$ are shown in Figure 1a and 1b, respectively. All n-channel OFETs were fabricated on heavily doped n^{++} Si using top-contact geometry. Thermally grown SiO_2 (200-nm thick) was used as the gate dielectric. The TiO_x injection layer was inserted between source–drain electrodes and the active semiconducting layer as shown in Figure 1c. The TiO_x layer was prepared using sol–gel chemistry as described in detail elsewhere.[11–13]

Enhanced n-channel performance is clearly seen in the output characteristics, as shown in Figure 2. The data in Figure 2 indicate

[*] Dr. S. Cho, Dr. J. H. Seo, Prof. A. J. Heeger
Center for Polymers and Organic Solids
University of California at Santa Barbara
Santa Barbara, CA 93106-5090 (USA)
E-mail: sucho@physics.ucsb.edu; ajhe@physics.ucsb.edu
Prof. K. Lee
Department of Materials Science & Engineering
Gwangju Institute of Science and Technology
Gwangju 500-712 (Korea)
E-mail: klee@gist.ac.kr

DOI: 10.1002/adfm.200900189

that (for both $PC_{61}BM$ and $PC_{71}BM$) the saturation currents are higher in FETs with the TiO_x layer by as much as an order of magnitude. For the devices without the TiO_x layer, there is clear evidence of non-ohmic behavior at low source-drain voltages (V_{ds}) implying a complex metal-semiconductor interface with high contact resistance. At high gate bias (V_{gs}) and low V_{ds}, leakage currents dominate. These undesired characteristics near $V_{ds} \approx 0$ are not observed in otherwise identical devices fabricated with a TiO_x layer.

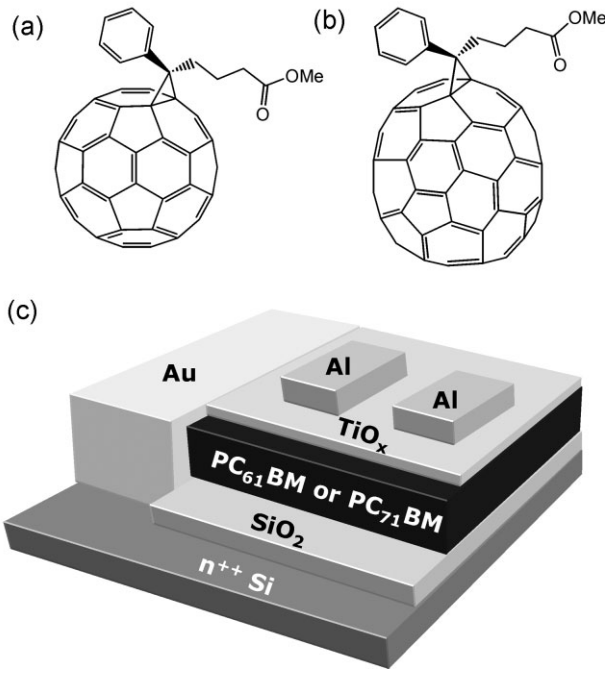

Figure 1. Molecular structures of a) $PC_{61}BM$ and b) $PC_{71}BM$. c) Schematic diagram of a top contact n-type field-effect transistor fabricated using $PC_{61}BM$ or $PC_{71}BM$ with TiO_x injection layer.

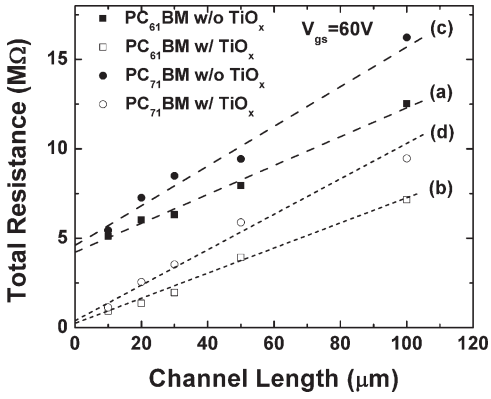

Figure 3. Total resistance between the source and drain electrodes ($R_{total} = R_c + R_{ch}$) as a function of the channel length (L). a) $PC_{61}BM$ FET without TiO_x injection layer (■), b) $PC_{61}BM$ FET with TiO_x injection layer (□), c) $PC_{71}BM$ FET without TiO_x injection layer (●), and d) $PC_{71}BM$ FET with TiO_x injection layer (○).

The contact resistances between the fullerene n-type semiconductor and the electrodes (source and drain) clearly limit the FET performance. Figure 3 shows the results of measurements of total resistance between the source and drain (R_{total}) as a function of the channel length (L), as obtained from the linear portion of I_{ds}–V_{ds} curves for various L ($V_{gs} = 60$V). Since the channel resistance is proportional to L, the contact resistance (R_c) can be obtained from extrapolation of R_{total} *vs.* L to zero channel length. The results show that devices with a TiO_x layer have lower R_{total} values and that R_{total} extrapolates to $R_c \approx 0.3$ MΩ for $PC_{61}BM$ FET, ≈0.4 MΩ for $PC_{71}BM$ FET at $L = 0$. Note that the slope of the R_{total} *vs.* L line did not change by introducing TiO_x layer in either $PC_{61}BM$ FETs or $PC_{71}BM$ FETs, implying that the true channel resistances are unaffected by the addition of the TiO_x layer.

Figure 4 shows the transfer characteristics, I_{ds} *vs.* V_{gs}, of OFETs fabricated with $PC_{61}BM$ (Fig. 4a) and $PC_{71}BM$ (Fig. 4b) with and without a TiO_x injection layer. Data obtained from similar OFETs with Ca electrodes are also included for comparison. The transport data are typical of n-channel OFETs; the devices turn on with positive gate bias. Comparison of device characteristics fabricated with and without a TiO_x injection layer indicates that insertion of a TiO_x layer yields an increase in I_{ds} by approximately an order of magnitude of values approaching those obtained using Ca electrodes. As demonstrated above, the lower I_{ds} values obtained without the TiO_x layer result from the high contact resistance, rather than from reduced electron mobility.

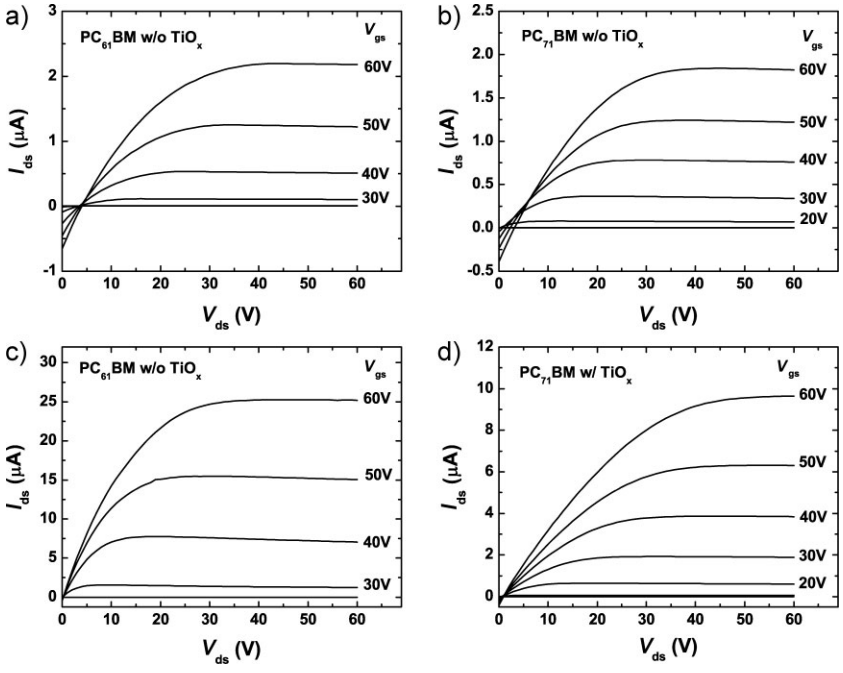

Figure 2. Output characteristics of the n-type a) $PC_{61}BM$ FET without TiO_x layer, b) $PC_{71}BM$ FET without TiO_x layer, c) $PC_{61}BM$ FET with TiO_x layer, and d) $PC_{71}BM$ FET with TiO_x layer.

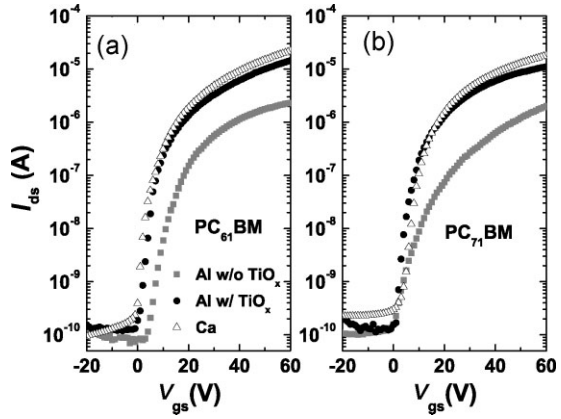

Figure 4. Transport characteristics of the n-type a) $PC_{61}BM$ FET and b) $PC_{71}BM$ FET with (●) and without (■) TiO_x injection layer. The results obtained from the devices fabricated with Ca electrodes (▲) are given for comparison.

Figure 5 shows a schematic diagram of potential profile between source and drain. The dashed line is an ideal linear potential profile as would be obtained in the uniform channel approximation with $R_c = 0$. When V_{ds} becomes comparable to the gate voltage, pinch-off occurs and I_{ds} saturates. Under these conditions, the standard equation for the transconductance is valid;

$$I_{ds} = [\mu C_i(W/2L)](V_{gs} - V_{th})^2 \quad (1)$$

where W is the channel width, L is the channel length of the devices, C_i is the capacitance (per unit area) of dielectric layer, and V_{th} is the threshold voltage. When Equation 1 is valid, one can obtain the transport mobility from the dependence of $(I_{ds})^{1/2}$ on the gate voltage (V_{gs}) with the standard equation

$$(I_{ds})^{1/2} = [\mu C_i(W/2L)]^{1/2}(V_{gs} - V_{th}) \quad (2)$$

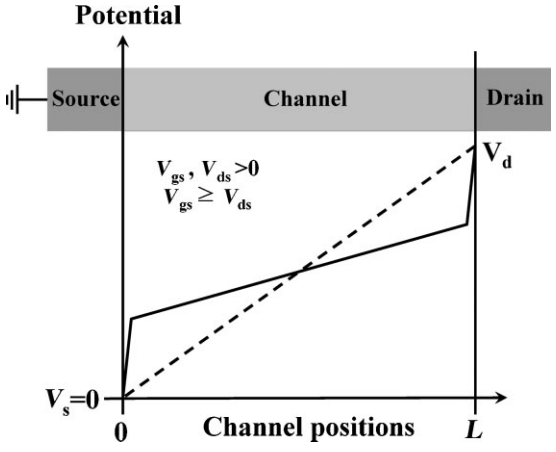

Figure 5. Schematic diagram of hypothetical channel potential profile. The dashed line is the ideal (no contact resistance) linear potential profile. Solid line is the predicted potential profile of the FET with serious contact resistance.

Note that the extracting mobility from the Equation 2 only yields a mean value that does not account for possible gate-voltage dependence.

Mobility values obtained under these conditions are close to the intrinsic transport mobilities. On the other hand, for a device in which the contact resistance is significantly larger than the true channel resistance (see Figs. 4 and 5), Equation 1 is not valid. Therefore, for FETs with high contact resistance, Equation 2 is not applicable, and one simply cannot infer a mobility from a plot of $(I_{ds})^{1/2}$ *vs.* V_{gs}. There are many examples in the literature that report an apparent correlation between contact resistance and mobility.[1,14–18] In fact, the mobility values inferred from FETs in which the contact resistance is large are simply not meaningful.

For FETs with a TiO_x layer, the contact resistance is small, Equation 2 is valid, and the electron mobilities are properly obtained from the linear plot of $(I_{ds})^{1/2}$ vs. V_{gs}: $\mu_1 = 2.8 \times 10^{-2}$ cm^2 V^{-1} s^{-1} for the $PC_{61}BM$ and $\mu_2 = 2.2 \times 10^{-2}$ cm^2 V^{-1} s^{-1} for the $PC_{71}BM$; nearly the same as the mobility values obtained from devices fabricated with Ca electrodes (3.5×10^{-2} cm^2 V^{-1} s^{-1} for the $PC_{61}BM$ and 3.7×10^{-2} cm^2 V^{-1} s^{-1} for the $PC_{71}BM$). We note, in addition, that for $PC_{61}BM$, the threshold gate voltage was reduced from approximately 5 V to nearly zero.

The effect of TiO_x injection layer appears to be quite general. Figure 6 shows measured contact resistances obtained from devices with different metals (Ag, Al, Cr, Au) with different work functions. For the devices without a TiO_x layer, the measured R_c values increase with increase in the work function, implying an increase in the height of the energy barrier between the fullerene semiconductor and the metal contact. For FETs with a TiO_x layer, R_c values are lower and the sensitivity to the metal work function nearly disappears (Au gives a slightly higher R_c than the other metals).

Figure 7 shows the fullerene mobilities obtained from OFETs fabricated with a TiO_x injection layer and with a series of metals with different work functions. With the TiO_x injection layer, the measured mobilities are relatively insensitive to the work function of the source/drain metals and, again, close to the maximum values obtained from devices fabricated with Ca electrodes.

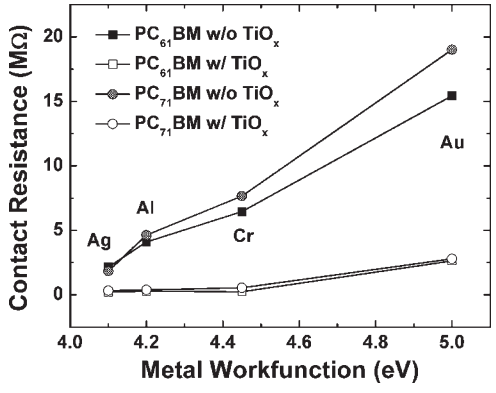

Figure 6. Contact resistance of the n-type $PC_{61}BM$ FET and $PC_{71}BM$ FET (with and without TiO_x) fabricated with various source and drain electrodes. The inset shows the data obtained from the devices with TiO_x layer on an expanded scale.

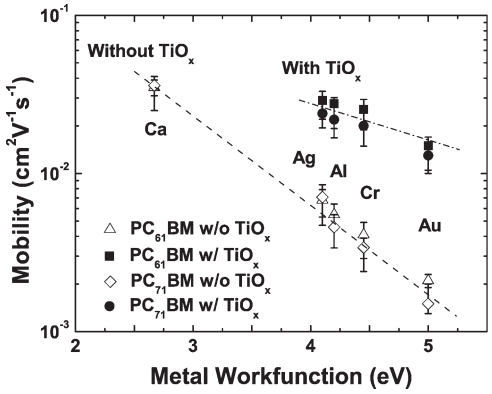

Figure 7. Electron mobilities of the n-type $PC_{61}BM$ FET and $PC_{71}BM$ FET (with and without TiO_x) fabricated with various source and drain electrodes. Because of the high contact resistance, the mobilities obtained from Equation 2 for FETs fabricated are not valid. The apparent values obtained without TiO_x are shown only to demonstrate the potential for serious error (approximately an order of magnitude too small).

In order to more directly probe the electronic energy shifts resulting from the TiO_x layer, we carried out UPS measurements on the $PC_{61}BM/TiO_x$ and $PC_{71}BM/TiO_x$ bilayer structures. Figure 8 shows the UPS spectra taken from TiO_x, $PC_{61}BM$, $PC_{71}BM$, $PC_{61}BM/TiO_x$ and $PC_{71}BM/TiO_x$. The Fermi energy (E_F) was determined from the Al surface and all other spectra are plotted with respect to this value. The normalized secondary edges of all films are shown in Figure 8a. The vacuum levels (VLs) of the samples were determined by linear extrapolation of secondary electron cutoffs on the high binding energy side of the UPS spectra (15–18 eV). The secondary edges shift toward higher binding energy for the TiO_x, while toward lower binding energies for the $PC_{61}BM$ and $PC_{71}BM$ without the TiO_x layer. Since the VL shift indicates the magnitude of the interfacial dipole, the UPS spectra suggest that the TiO_x induces a relatively strong interfacial dipole (VL shift of TiO_x is 0.5 eV). In general, the presence of such an interfacial dipole affects the band alignment at the interface; decreasing VL induces a downward shift of the whole band structure.[19]

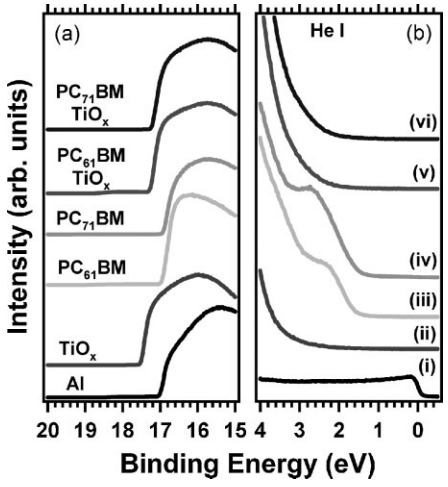

Figure 8. UPS spectra of i) Al, ii) TiO_x, iii) $PC_{61}BM$, iv) $PC_{71}BM$, v) $PC_{61}BM/TiO_x$ and vi) $PC_{71}BM/TiO_x$. a) High binding energy cutoff region; b) the HOMO onset region.

Figure 8b shows the highest occupied molecular orbital (HOMO) onset for TiO_x, $PC_{61}BM$, $PC_{71}BM$, $PC_{61}BM/TiO_x$, and $PC_{71}BM/TiO_x$. Comparing the shift in the HOMO onset to E_F of Al provides the relative position of the HOMO level. The ionization potential (IP) was determined by using the incident photon energy ($h\nu$), the secondary cutoff and the onset of the HOMO.[20] We found the following IP values: 7.21 eV for TiO_x, 5.84 eV for $PC_{61}BM$, and 5.87 eV for the $PC_{71}BM$. The IP of $PC_{61}BM$ agrees well with the literature value.[21] For the samples with TiO_x layer, the HOMO onsets of $PC_{61}BM$/TiOx and $PC_{71}BM/TiO_x$ shift toward higher binding energies relative to those of $PC_{61}BM$ and $PC_{71}BM$ single layer. In other words, the TiO_x layer increases the HOMO energies of $PC_{61}BM$ and $PC_{71}BM$.

Energy level diagrams for the $PC_{61}BM$, $PC_{71}BM$, $PC_{61}BM/TiO_x$, and $PC_{71}BM/TiO_x$ as inferred from the UPS data are illustrated in Figure 9. The values shown for each HOMO and LUMO indicate the energy difference from the E_F of Al. The energy differences from the E_F of Al to the HOMO of $PC_{61}BM$ and $PC_{71}BM$ are 1.59 eV and 1.54 eV, respectively. Since the LUMO level is estimated by using the HOMO and the measured optical gaps, the electron injection barriers from Al to the LUMO level are estimated as 0.61 eV for the $PC_{61}BM$ and 0.66 eV for the $PC_{71}BM$. The electron injection barriers decrease after introdu-

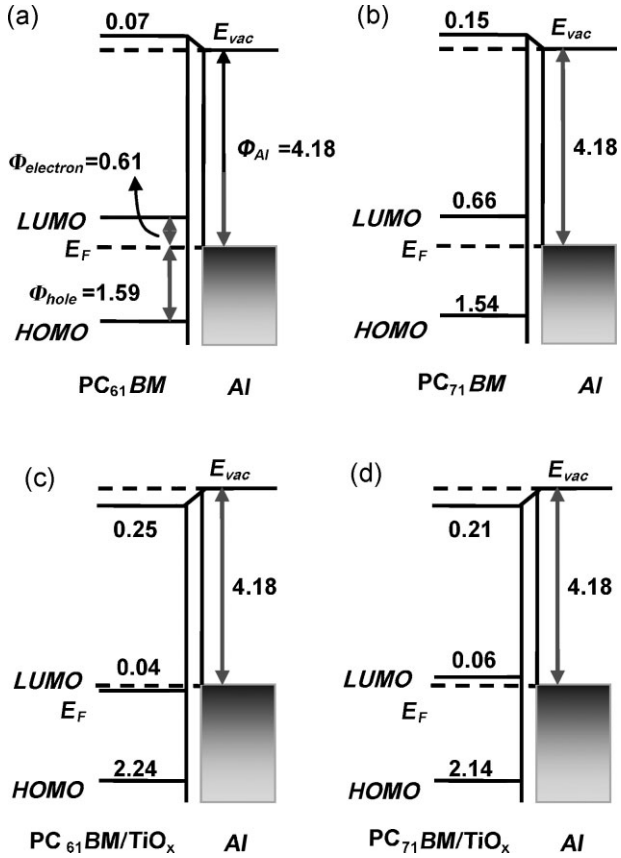

Figure 9. Energy level diagrams for the a) $PC_{61}BM$, b) $PC_{71}BM$, c) $PC_{61}BM/TiO_x$, and d) $PC_{71}BM/TiO_x$, obtained from the UPS data.

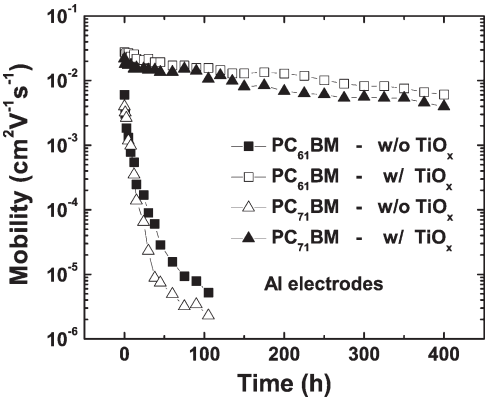

Figure 10. Comparison of the mobilities obtained from n-type $PC_{61}BM$ FET and $PC_{71}BM$ FET (with and without TiO_x) as a function of storage time in air.

cing the TiO_x injection layer. The electron injection barriers decrease to –0.04 eV for the $PC_{61}BM/TiO_x$ and to 0.06 eV for the $PC_{71}BM/TiO_x$. These reductions in the electron injection barriers result from relatively strong interfacial dipole at the surface of the TiO_x layer. Note that we used the measured optical gap to determine the LUMO energies. Typically, the optical gap is smaller than transport gap because it does not take into account the exciton binding energy. Thus, the true transport gap might be slightly higher than the LUMO level estimated using optical gap.

The TiO_x layer also acts as a passivating layer that protects the FET and inhibits degradation of device performance from air exposure.[13] Figure 10 shows the electron mobility obtained from FETs fabricated with $PC_{61}BM$ and $PC_{71}BM$ as a function of exposure time in air. The mobilities of both $PC_{61}BM$ and $PC_{71}BM$ FET without TiO_x layer decreased rapidly (by almost four orders of magnitude) when exposed to air for only 100 hours. The electron mobility obtained from devices with the TiO_x layer shows a decrease of less than one order of magnitude over the same exposure period. Even after 400 hours in air, the electron mobility remains at approximately $10^{-3}\,cm^2\ V^{-1}s^{-1}$. In our previous report, a TiO_x layer was deposited on top of the FET (rather than between the electrodes and the fullerene as reported here).[13] The results described here demonstrate that the TiO_x layer inserted between the electrodes and the fullerene acts as an electron injection layer and also inhibits degradation caused by O_2 and H_2O.

3. Conclusions

In conclusion, we have studied the performance of n-channel OFETs fabricated with the soluble fullerenes $PC_{61}BM$ and $PC_{71}BM$ as the semiconductor in the channel. Improved injection is achieved by introducing an electron injection layer using solution-processible TiO_x. With the TiO_x injection layer, the electron mobilities in FETs fabricated with Al electrodes $\mu_1 = 2.8 \times 10^{-2}\,cm^2\ V^{-1}\ s^{-1}$ for the $PC_{61}BM$ FET and $\mu_2 = 2.2 \times 10^{-2}\,cm^2\ V^{-1}\ s^{-1}$ for the $PC_{71}BM$ FET. Moreover, the TiO_x layer essentially eliminates the contact resistance between the electrodes and the fullerene layer in the channel. UPS studies demonstrate that the inserted TiO_x layer induces a decrease in the electron injection barrier implying the existence of a relatively strong interfacial dipole. The TiO_x layer also serves to protect the device against penetration of O_2 and H_2O into active layer, and thereby leads to a significant improvement in the lifetime of OFETs when exposed to air.

4. Experimental

N-type FETs (with the top contact geometry) were fabricated on heavily doped n-type Si wafers each covered with a thermally grown SiO_2 layer with thickness of 200 nm. The active layer was deposited by spin-casting at 2000 rpm. $PC_{61}BM$ and $PC_{71}BM$ solutions were prepared at 1.0 wt% concentration in chloroform. The thickness of the fullerene films was about 60 nm. Prior to deposition of source-drain electrodes, the films were dried on hot plate stabilized at 80°C for 30 minutes. The fullerene deposition was carried out in the glove box filled with N_2.

After deposition of the fullerene film, the samples were taken out from glove box into air to deposit TiO_x layer. The TiO_x solution (1:150 diluted from the initial product) was spin-cast in air on top of the fullerene layer with thicknesses typically in the range 10–15 nm. Subsequently, the films were heated at 80 °C for 10 minutes in air to remove the solvent.

Source and drain electrodes were deposited by thermal evaporation using a shadow mask. The thickness of source and drain electrodes was 50 nm. Channel length (L) and channel width (W) were 50 μm and 1.5 mm, respectively. Electrical characterization was performed using a Keithley semiconductor parametric analyzer (Keithley 4200) under N_2 atmosphere.

Ultra thin bilayer samples for UPS measurements were prepared by spin-coating on SiO_2/Si substrates covered with Al metal (100 nm). The fullerene layer was deposited by spin-casting (4000 rpm, 60s) using 0.2 wt% solution in chloroform. The TiO_x layer was then deposited on top of the fullerene thin film by spin-coating in air using a highly diluted TiO_x solution (1:500). Typical thicknesses of the fullerene films ~2.0 nm and the thickness of TiO_x layer was ~1.5–2 nm.

The UPS analysis chamber was equipped with a hemispherical electron energy analyzer (Kratos Ultra Spectrometer) and was maintained at 1×10^{-9} Torr. The UPS measurements were carried out using the He I ($h\nu = 21.2$ eV) source. During UPS measurements, a sample bias of −9 V was used in order to separate the sample and the secondary edge for the analyzer. Samples were also kept in a high vacuum chamber overnight to remove residual solvent. In order to confirm reproducibility of the UPS spectra, we repeated the measurements twice on three sets of samples.

Acknowledgements

This work was supported by the Heeger Center for Advanced Materials at the Gwangju Institute of Science and Technology, by the Global Research Laboratory Program of the Korean Government (M60605000005-06A0500-00510), and by the Samsung Advanced Institute of Technology. The UPS data were obtained by use of the facilities provided by the California Nanosystems Institute (CNSI) at UCSB.

Received: February 3, 2009
Published online:

[1] *Organic field-effect transistors* (Eds: Z, Bao, J. Locklin), CRC Press, Boca Raton, FL **2007**.
[2] C. Waldauf, P. Schilinsky, M. Perisutti, J. Hauch, C. J. Brabec, *Adv. Mater.* **2003**, *15*, 2084.
[3] S. P. Tiwari, E. B. Namdas, V. R. Rao, D. Fichou, S. G. Mhaisalkar, *IEEE Electron Device Letters* **2007**, *28*, 880.
[4] T. W. Lee, Y. Byun, B. W. Koo, I. N. Kang, Y. Y. Lyu, C. H. Lee, L. Pu, S. Y. Lee, *Adv. Mater.* **2005**, *17*, 2180.

[5] P. H. Wöbkenberg, D. D. C. Bradley, D. Kronholm, J. C. Hummelen, D. M. de Leeuwd, M. Cölle, T. D. Anthopoulos, *Synth. Met.* **2008**, *158*, 468.
[6] T. D. Anthopoulos, D. M. de Leeuw, E. Cantatore, P. van't Hof, J. Alma, J. C. Hummelen, *J. Appl. Phys.* **2005**, *98*, 054503.
[7] L.-L. Chua, J. Zaumsell, J.-F. Chang, E. C.-W. Ou, P. K.-H. Ho, H. Sirringhaus, R. H. Friend, *Nature* **2005**, *434*, 194.
[8] Th. B. Singh, N. Marjanović, P. Stadler, M. Auinger, G. J. Matt, S. Günes, N. S. Sariciftci, *J. Appl. Phys.* **2005**, *97*, 083714.
[9] T. Mori, H. Fujikawa, S. Tokito, Y. Taga, *Appl. Phys. Lett.* **1998**, *73*, 2763.
[10] S. Hoshino, S. Nagamatsu, M. Chikamatsu, M. Misaki, Y. Yoshida, N. Tanigaki, K. Yase, *Jpn. J. Appl. Phys.* **2002**, *41*, 808.
[11] J. Y. Kim, S. H. Kim, H.-H. Lee, K. Lee, W. Ma, X. Gong, Alan, J. Heeger, *Adv. Mater.* **2006**, *18*, 572.
[12] J. Y. Kim, K. Lee, N. E. Coates, D. Moses, T.-Q. Nguyen, M. Dante, A. J. Heeger, *Science* **2007**, *317*, 222.
[13] S. Cho, K. Lee, A. J. Heeger, *Adv. Mater.* **2009**, DOI: 10.1002/adma.200803013.
[14] D. Natali, L. Fumagalli, M. Sampietro, *J. Appl. Phys.* **2007**, *101*, 014501.
[15] G. Horowitz, P. Delannoy, *J. Appl. Phys.* **1991**, *70*, 469.
[16] C. Goldmann, S. Haas, C. Krellner, K. P. Pernstich, D. J. Gundlach, B. Batlogg, *J. Appl. Phys.* **2004**, *96*, 2080.
[17] S. Weng, C. Kuo, S. Wu, *J. Polym. Res.* **2003**, *10*, 211.
[18] S. Scheinert, G. Raasch, *J. Appl. Phys.* **2009**, *105*, 014509.
[19] J. H. Seo, T.-Q. Nguyen, *J. Am. Chem. Soc.* **2008**, *130*, 10042.
[20] W. R. Salaneck, M. Lögdfund, M. Fahlman, G. Gresinski, Th. Kugler, *Mater. Sci. Eng.* **2001**, *R34*, 121.
[21] K. Akaike, K. Kanai, H. Yoshida, J. Tsutsumi, T. Nishi, N. Sato, Y. Ouchi, K. Seki, *J. Appl. Phys.* **2008**, *104*, 023710.